Heterodyne interferometer for triggering gas-puff PRSs

Final Report

Contract #: DTRA01-03-P-0241

Prepared By:

Robert C. Hazelton

HY-Tech Research Corp.

Radford, VA 24141

Prepared For:

Mr. Randy Davis

Defense Threat Reduction Agency

Alexandria, VA 22310

May 25, 2004

REPORT DOCUMENTATION PAGE

Form Approved
OMB No. 0704-0188

PLEASE DO NOT RETURN YOUR FORM TO THE ABOVE ADDRESS.

1. REPORT DATE *(DD-MM-YYYY)*	2. REPORT TYPE	3. DATES COVERED *(From - To)*
25-05-2004	Technical	29-09-2003 to 25-05-2004

4. TITLE AND SUBTITLE
Heterodyne Interferometer for Triggering Gas-Puff PRSs

5a. CONTRACT NUMBER
DTRA01-03-P-0241

5b. GRANT NUMBER

5c. PROGRAM ELEMENT NUMBER
0605502BR

6. AUTHOR(S)
Robert C. Hazelton

5d. PROJECT NUMBER
BB

5e. TASK NUMBER
AA

5f. WORK UNIT NUMBER
10736

7. PERFORMING ORGANIZATION NAME(S) AND ADDRESS(ES)
HY-Tech Research Corporation
104 Centre Court
Radford, Virginia 24141

8. PERFORMING ORGANIZATION REPORT NUMBER
N/A

9. SPONSORING/MONITORING AGENCY NAME(S) AND ADDRESS(ES)
Defense Threat Reduction Agency
8725 John J. Kingman Road, MSC 6201
Fort Belvoir, VA 22060-6201

TDNS/R. Davis

10. SPONSOR/MONITOR'S ACRONYM(S)
DTRA

11. SPONSOR/MONITOR'S REPORT NUMBER(S)
N/A

12. DISTRIBUTION/AVAILABILITY STATEMENT
Distribution Statement A - Approved for Public Release; distribution is unlimited.

13. SUPPLEMENTARY NOTES
This work was sponsored by the Defense Threat Reduction Agency.

14. ABSTRACT
Consistent timing between the injection of gas in plasma radiation sources (PRSs) and the generator current pulse is crucial to producing high-yield x-ray pulses. This Phase 1 SBIR effort has shown that triggering modes currently used in DTRA's x-ray simulator program (high voltage trigger pin; command fire mode) introduce an effective variation in initial load mass of +/-11%, and this may be as high as +/-20%. This variation is so large that it can completely mask any PRS improvement attempted in the x-ray simulator R&D program, and result in approx. 20% variation in x-ray yield. This effort demonstrated the utility of a compact, heterodyne interferometer trigger system to reduce effective variation in load mass, where variations as low as +/-1.5% may be possible. The interferometer system can monitor the gas puff time history, with resulting data used to improve the density profile of each simulator shot. It will also help to quantify the amount of pre-ionization and early electron density buildup for the plasma radiation sources.

15. SUBJECT TERMS
laser interferometer; plasma radiation source; x-ray simulation.

16. SECURITY CLASSIFICATION OF:			17. LIMITATION OF ABSTRACT	18. NUMBER OF PAGES	19a. NAME OF RESPONSIBLE PERSON
a. REPORT	b. ABSTRACT	c. THIS PAGE			19b. TELEPHONE NUMBER *(Include area code)*

I. Executive Summary

Large X-ray generators using gas fill loads are an important element in the DTRA simulator program. Consistent relative timing between the injection of the gas shell and the generator current pulse is crucial to producing consistent, high-yield x-ray pulses. This study has shown that the two common triggering modes currently used introduce an average variation in the initial load mass of ± 11 % with peak exertions reaching ± 20%. The scaling laws for the yield in the I^4 regime indicate that this variation in load mass can result in • 20% variation in the average yield with significantly larger peak variations. HY-Tech had developed a compact heterodyne interferometer based trigger generator to replace existing high voltage trigger pin technology and command fire modes currently used. The innovative features include the implementation of an all fiber optic system in conjunction with a novel multipass load cell to increase sensitivity and reduce noise susceptibility. The optical components of the load cell are mounted on a compact base which attaches to the anode plate without obstructing any line-of-sight ports currently used. The modular design allows the load cell to be easily removed, by disconnecting the optical fibers, for cleaning of the insulator stack and replaced afterward without disturbing the alignment of the optical components. The interferometer also acts as a monitor to provide an absolute time history of the gas puff which can then be manipulated to give an axial line density profile for each simulator shot. It will also provide a measure of the pre-ionization level as well as the early electron density buildup during the generator pulse.

The implementation of this trigger system on current and future simulators should result in an initial load mass variation of • 1.5% which is determined by the noise level in the detector system. Jitter in the erection of the Mark banks introduces an insignificant mass variation, which would be measured by the system and therefore known. The DTRA simulator program is benefited in two ways when the load mass variation is removed as a source of variation in the simulator yield. DTRA could assure users that a more consistent on target fluence can be achieved than is currently available and the effect of intentional variations in load configurations, such as number of return current rods, can be determined using fewer generator shots.

The two overriding technological challenges to developing an interferometer based trigger system was to obtain sufficient sensitivity to provide a reliable trigger signal while suppressing background phase noise introduced by environmental vibrations and long term drifts induced by temperature variations in the optical components. An eight-pass load cell was used to obtain the desired sensitivity. A 1cm x 1cm area is traversed by the 8 beams which averages any sharp spatial variations in gas density. Vibrational effects are minimized by transmitting the scene beam and the frequency shifted reference beam as two orthogonally polarized beams down the same polarization preserving fiber up to the load cell inside the vacuum chamber. A polarizing beam splitter separates the reference beam which propagates down fibers located on the load cell from the scene beam. The two are recombined on the load cell and transmitted through a multi mode fiber to the screen room where they are analyzed. Phase variation induced by mechanical vibration are minimized in this common mode configuration where the scene and reference beams are subject to the same stresses. Long term thermal drifts are minimized using a novel voltage controlled oscillator with a feedback sensor to maintain a zero reference until the measurement is begun. The required coherence length was achieved in an inexpensive HeNe laser using a simple temperature control system to maintain single longitudinal mode operation in the laser. The use of this laser system allowed the operation of an eight-pass cell with a 6m path imbalance between the scene and reference beams with no loss of coherence.

The trigger system was tested on the gas puff produced by a puff-on-puff Double-EAGLE (DE) nozzle that was loaned to HY-Tech by Titan Pulse Sciences Division. Measurements made at conditions approximately those used on DE indicate a $\pm 2°$ phase uncertainty, due to noise, when the total phase shift was 130°, which corresponds to a percent variation in mass of 1.5%. These measurements show that a standard deviation of $\pm$ 12% would have occurred in the load mass if the generator was fired a fixed time after the gas puff, in the command fire mode. A comparable average variation of 11% would have occurred if a high voltage break down pin were used to trigger the generator. These mass variations would result in a yield variation of $\pm$ 24% and $\pm$ 22% in the two cases. Since the minimum load mass observed was 50% of the maximum value recorded for ostensibly the same trigger conditions, it is clear that these load mass effects can

completely mask any effect on the yield which could be due to optimization studies. Elimination of these variations in load mass would make it easier to evaluate the effects of preionization, mass distribution, and the number of return current rods.

This Phase I study has shown that a compact, easy to use heterodyne interferometer based system can be built for reliably and reproducibly triggering the pulse power system driving a gas puff load. A stable system can be built using relatively inexpensive optical components. The implementation of this trigger system on radiation simulators will reduce the costs of improving load performance and result in a more consistent source of radiation for users.

II. Introduction

The purpose of this program was to develop a triggering system based upon the direct measurement of the mass loading of gas fill loads for plasma radiation source (PRS) x-ray simulators used by the DTRA community. Triggering methods presently used are to command fire the entire system from a series of externally generated timing pulses or to use the signal from a high voltage breakdown pin located in the gas puff nozzle. In our study and the studies of others using the Titan Pulsed Science 1234 puff valve it was found that, even in the breakdown pin triggered mode, the shot-to-shot mass loading had a standard deviation of • 12% and a total range of • 22%. We have developed a heterodyne laser interferometer which can be used to monitor the mass loading of each shot (in situ) and provide a timing signal that will be able to reproduce the mass loading within 1.5%. Given the limited shot rate of the major x-ray simulators, we expect that the shot-to-shot repeatability will be greatly improved. This will not only allow DTRA to better serve the user community, but it will also enhance DTRA's effort to characterize and optimize the function of PRS sources.

In our original proposal, we delineated four technical objectives which must be met for the successful completion of the Phase I effort. They are:

- Implement a heterodyne interferometer in a Michelson format using fiber optic components.
- Interface the interferometer with a novel multi-pass test cell.
- Ascertain vibrational noise levels and implement design changes to minimize these levels.

- Implement novel detector circuit designed to generate a reliable and reproducible trigger signal.

The final product is the system shown in Fig. 1. The system can best be broken down into three functional components; the modulated laser source and delivery system; the interferometer head and; the detection and demodulation system. Several innovations were required in the course of the program to arrive at the system depicted in Fig. 1.

Laser source and delivery system

In a typical heterodyne interferometer, an acousto-optic modulator (or Bragg cell) is used to produce and separate two laser beams, one of whose frequency is shifted by the Bragg cell frequency, f_b. Usually, at this juncture one beam is used as a scene beam and one is used as a reference beam in some standard interferometer configuration. In our application, the two laser beams must be transmitted from the laser, in the screen room, to the head, located inside the PRS chamber. An innovative fiber optic technique is used to accomplish this with minimal phase noise. We take the shifted beam and rotate the polarization 90• and then recombine it with the unshifted beam. The axes of the two beams are then aligned with the orthogonal axes of a polarization preserving fiber (PPF) optic cable. Because of the unique characteristics of a PPF, the two beams can travel independently through the same fiber to the interferometer head. They are subject to identical stresses and, therefore, incur identical phase noise which cancels at the detector. Since the laser beams can be carried over long distances, the laser source can be conveniently located in a screen room. The fiber optic cable can be easily routed to the simulator without having to propagate laser beams in free space, removing any interference or safety issues.

Interferometer head

Because of the innovative beam delivery system, the interferometer head can actually be situated inside the simulator vacuum chamber, very close to the load. At the interferometer the laser beams are extracted from the fiber and recollimated. Again, because of the unique properties of the PPF the two laser beams can be separated using a polarizing beamsplitter. The interferometer is set up as a Michelson interferometer configuration. The reference arm consists of a single mirror while the scene beam makes many passes through the load region using an innovative load cell consisting of two right

angle prisms, as shown in Fig. 1. By simply translating the far prism, the number of passes can be controlled in increments of two. The multi-pass cell accomplishes two things. First, it increases the sensitivity of the system by increasing the total path affected by the presence of the gas puff. Second, by distributing the path throughout the gas puff, one can average over any local nonuniformities that would give an erroneous measure of the total mass loading. The geometry shown which averages over the load diameter can be reconfigured to average over the shell thickness (1cm) or over an axial length. In each arm of the interferometer head there is a polarization rotator that results in a total rotation of 90•. When these beams return to the polarizing beam splitter, they are directed at right angles to their original paths. The recombined beams are then launched into a multi-mode fiber optic cable, which then carries them back to the detection and demodulation system in the screen room.

The modular design provides several important features. A very compact head can be fabricated on one continuous optical surface maintaining component alignment and affording very good vibrational immunity. It can be easily dismounted and removed by simply detaching the two fiber optic cables. Reinstallation with minimal realignment is straightforward and simple, minimizing any impact on the timely operation of the entire system. The fiber optic connections eliminate the need to use diagnostic ports to transport the laser beams to and from the load region.

Detection and demodulation system.

When the recombined beams are detected by the photodiode, an output signal is detected at the beat frequency between the two optical frequency signals. In a standard heterodyne interferometer, the phase of this signal is compared with the phase of a reference signal derived from the Bragg cell driver. Due to path length differences and long term thermal drifts the actual phase difference is an indeterminate value. In most cases, the diagnostic is applied apostiori, and the unknown offset can be removed when the data is analyzed. The situation is different in our case where the data are used in real time and must be at zero phase at the time of arrival of the gas puff. In many commercial fiber optic interferometers this is accomplished by physically stretching the fiber used as the reference arm. This method is complex and in our configuration is not practical. To meet this need we designed and implemented a reference source consisting of a voltage

controlled oscillator (VCO) and a phase locked loop (PLL) feedback system. The system is capable of continuously changing the reference signal phase to keep the output phase at a zero level. The PLL control can then be disengaged just prior the gas puff arrival allowing the system to accurately track the phase induced by the gas starting at zero phase. In this way a trigger point can be consistently set which is representative of the desired mass loading, much as one would set an oscilloscope to trigger at a given signal level.

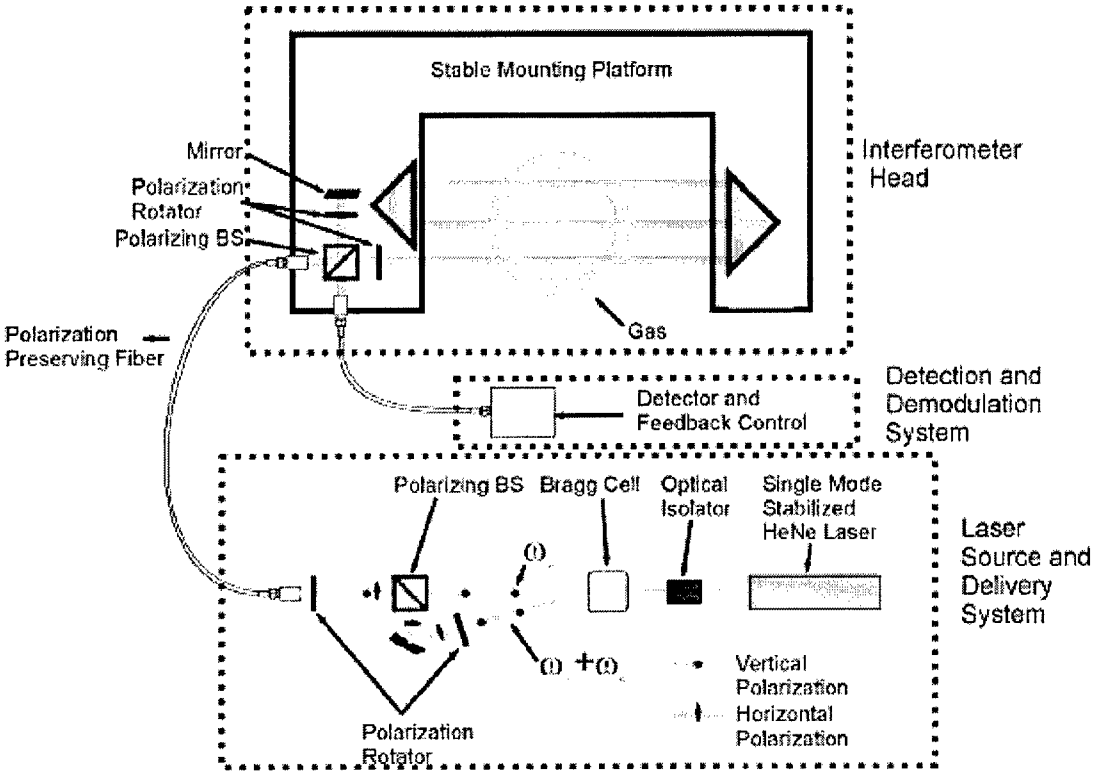

Figure 1. Schematic of complete heterodyne interferometer trigger system.

Development chronology

The overriding technological challenge to the development of a useful trigger interferometer was to overcome background phase noise introduced by environmental vibrations and other long term phase drifts induced by effects such as temperature variations. To this end the interferometer was designed and implemented in incremental steps to allow an independent assessment of environmental effects. In this way any

unexpected effects could be isolated and dealt with. As a first step, a simple interferometer was set up on a standard optical table to benchmark the baseline noise levels. Next a fiber delivery system was designed and tested. Although the proposal originally called for a two fiber approach with one fiber carrying the scene beam and another carrying the reference beam, a novel way was devised to carry both beams in the same single-mode, polarization preserving fiber. In the original plan the two beams in the two fibers would have been subject to similar stresses, while in this approach they are subject to identical stresses, thereby greatly reducing potential noise susceptibility. The system was tested in a balanced Michelson interferometer mode and showed substantial improvement over the benchmark tests. At this point we essentially had a working system to deliver the two beams to the simulator location. The next important feature is to return the recombined beams to a detector in a quiet environment. From previous experience we have learned that a recombined beam can be propagated along a multi-mode fiber without loss of coherent interference. In this case we used a 20 m segment of multi-mode fiber without any significant loss of detector signal. The final step was then to set up the multi-pass cell which is used to amplify the interferometer sensitivity. A double pass, unbalanced system was implemented with a 1.5 m path imbalance. Here a significant problem was encountered, in that the interferometer worked only periodically. After some investigation it was determined that standard commercial HeNe lasers did not have sufficient coherence length to operate properly because they typically operate with multiple longitudinal modes, with occasional single mode operation. To overcome this problem, we used a short tube HeNe that we had from other applications, and designed and implemented a feedback control system to maintain the laser in as stable, single longitudinal mode. The use of this laser system allowed us to set up and demonstrate the operation of an eight-pass cell (6m path imbalance) with no loss of coherence. The last design issue to be addressed was a method to compensate for long term drift effects and maintain the signal output at zero phase. The phase locked loop circuitry was designed and fabricated in conjunction with a voltage controlled oscillator. The circuit was tested and shown to maintain a zero output with about 2• accuracy.

Finally, a DE puff valve was obtained from Titan and installed in a HY-Tech vacuum chamber and the ability to measure the gas puff with high sensitivity was

demonstrated. Measurements of the mass loading based upon command firing or breakdown pin firing, exhibited a standard deviation of • 12 and • 11 % respectively. The extrema were • 22 and • 21% respectively. From low to high this represents a variation in mass loading of 50% for ostensibly the same trigger conditions. At this point, the optical interferometer was complete and tested

III. Experimental Results

Benchmark Testing

As a baseline experiment, a heterodyne interferometer was set up on an optical table with conventionally mounted optical components. As can be seen in Fig. 2, the background phase variations are a few times greater than our anticipated full scale signal from the gas puff of about 100-150•. Work progressed from here to reduce the noise to acceptable levels.

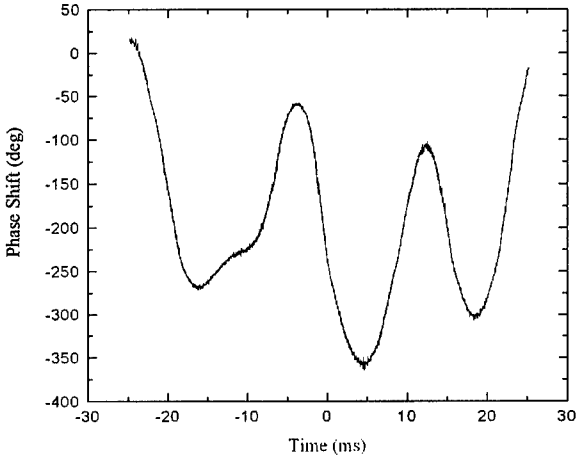

Figure 2. Phase noise in a conventional heterodyne interferometer set up on a good vibration isolation table.

Fiber Optic System Concepts

The basic geometry of the initially proposed, fiber optic, heterodyne interferometer is shown in Fig. 3. The approach is to build the system with fiber optic components to simplify the delivery and recovery of the laser beams to the simulator and limit

interference with other operations that would come from the use of free space laser beams. At the same time these components can be configured to minimize the impact of environmental noise.

The initial conceptual layout of the system is shown in Fig. 3 where the light from a HeNe laser is coupled to the single mode fiber input of the Bragg cell. The modulator produces two output beams, one at the original laser frequency and one offset by 40 MHz, each of which is coupled into a single mode fiber. Each of these fibers is, in turn, coupled to a fiber optic beam splitter. The pass-through beam of each splitter is then coupled to a nominal length (say 20 m) of single-mode fiber cable. These fibers represent the two legs of a Michelson interferometer. One fiber is terminated in a reflector and is the reference leg of the interferometer. The other fiber is launched into free space and is the scene leg of the interferometer. Here the scene beam enters a multi-pass optical cell with the gas load centered. This cell, which will be discussed in more detail, allows the laser beam to traverse the load region multiple times, effectively increasing the interferometer sensitivity. With proper alignment of the cell, the beam can be coupled back into the scene fiber. The return signals are split again and combined in the reference splitter and passed via fiber optic cable to the optical detector, which responds to the 40 MHz beat signal.

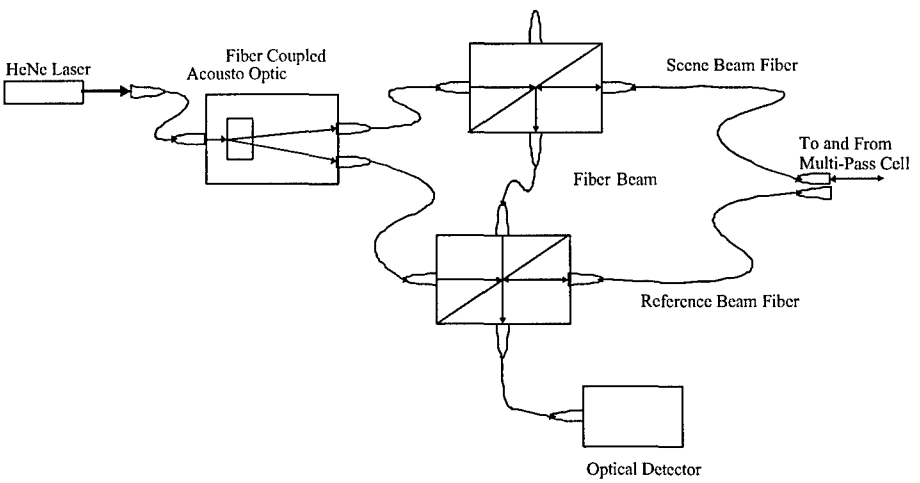

Figure 3. Initial concept of the heterodyne interferometer for use as a trigger generator.

The overriding issue in this program is the reduction in environmental noise (primarily phase shifts due to vibrational induced motion of optical components). In previous applications, we were viewing events on a microsecond time scale in which any vibration appeared as a small, linear signal which could be removed in the post-shot data analysis. Here the time scale has lengthened to milliseconds. Figure 2 represents a first concept of noise reduction, in which the scene and reference beams propagate along similar paths in similar fibers, with the hope that any vibrations will induce common mode noise which will cancel. After carrying out an extensive literature search for heterodyne and fiber optic interferometer concepts, we have modified the approach. Figure 4 shows the first step in this approach. Here the Bragg cell separates the two beams, one of which goes directly into a polarizing cube beamsplitter (PCBS). The other beam passes through a half wave plate to rotate its polarization 90•, and is then recombined with the other beam using the polarizing beam splitter. The recombined beams are then focused into a polarization preserving fiber optic cable such that one beam propagates along the fast axis of the cable and the other propagates along the slow axis. The important feature of the fiber optic is that the relative polarization of the two beams is maintained in the cable and therefore they can be again separated upon exiting the cable. In this manner the scene and reference beam experience nearly identical phase perturbations which cancel.

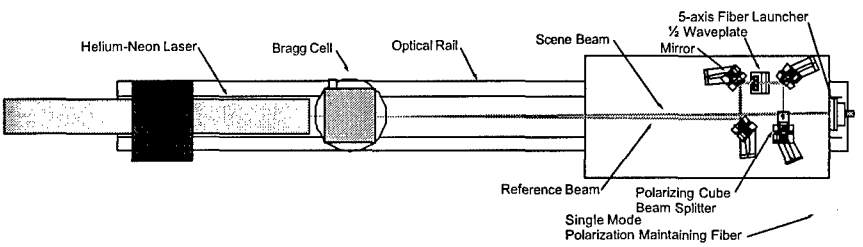

Figure 4. Updated concept of fiber optic delivery system in which both the scene and reference beams are carried in the same polarization preserving fiber optic cable.

The fiber launch system was fabricated and the system performance was incrementally tested. For the first test, the polarizing beam splitter was replaced by a nonpolarizing one and combined beams were fed into a detector. This setup is analogous

to the system previously tested with normal table top components in which the phase varied 400• over a 60 ms timeframe. Figure 5 shows the comparable output from the new setup. The signal has a high frequency component, which appears to be an electronic noise and a low frequency component that is caused by residual vibrations. The total signal has a standard deviation of 0.9•, while the vibrational component alone has a standard deviation of 0.3•. The latter figure represents a thousand-fold reduction in noise from the initial setup. The next step was to couple the combined beams into the polarization preserving fiber and measure any additional noise produced by the fiber. Figure 6 shows that the fiber introduces a small amount of additional noise up to a standard deviation of 0.7• over a 100 ms timeframe. One can see here a more long-term drift that contributes to this value.

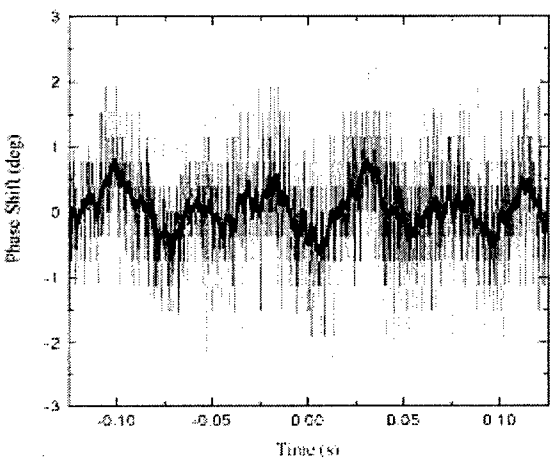

Figure 5. Phase noise produced on minature optical table use for combing orthognal beams and launching into polarization preserving fiber.

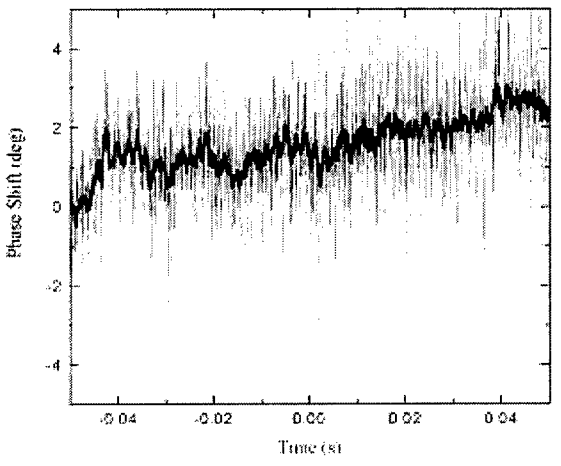

Figure 6. Phase noise with the addition of the polarization preserving fiber.

The next step was to set up the interferometer head as shown in Fig. 7. The basic arrangement is that of a Michelson interferometer. The mixed beam enters through the PPF where another polarizing beam splitter separates the shifted and unshifted components. Each passes through a quarter waveplate and is reflected by mirrors on each arm. Passing back through the waveplates completes a ninety-degree rotation of each beam, resulting in a single combined beam directed toward the 20-m multimode fiber optic cable. This fiber carries the light back to the detector system for measurement of the phase. Figure 8 shows the resulting phase noise for this configuration. The vibrational component has a standard deviation of 0.6•. This configuration demonstrates remarkable noise immunity. It is essentially one step away from the final configuration in which one arm of the interferometer is extended to form the multi-pass gas sensor.

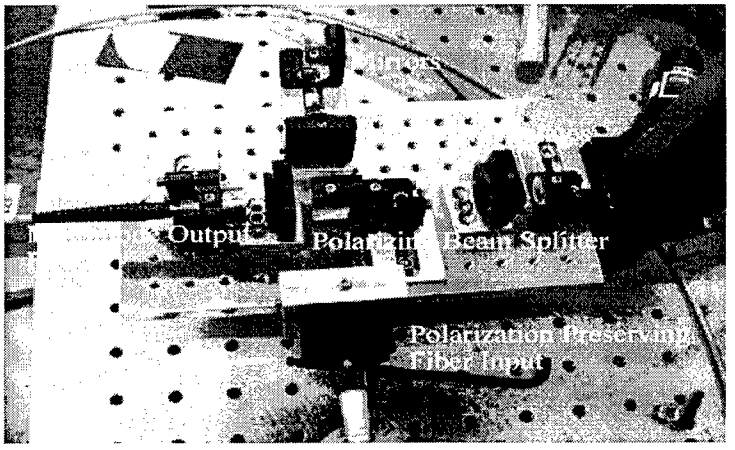

Figure 7. Interferometer head with a Michelson configuration.

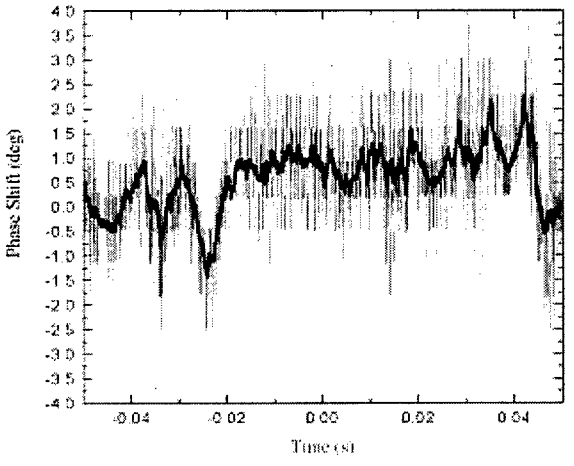

Figure 8. Phase noise with complete system in Michelson configuration.

Multi-pass Tests

The first steps were taken to test the multi-pass configuration. The first test consisted of extending one arm of the Michelson interferometer approximately 75 cm resulting in a path difference of 150-cm.

Here the results were inconsistent. Figure 9 shows a measurement that exhibited only a small increase in noise level from previous measurements with a balanced path setup. Here the total noise error is 1.8• while the low frequency error is 0.8•. In contrast, Fig. 10 shows the very next acquisition. Suddenly we were seeing steps of thousands of

degrees over the same time period. Changing lasers had no beneficial effect on the problem. A little investigation determined that the problem stemmed from the fact that typical HeNe lasers operate with multiple longitudinal modes and that the coherence length varies as the mode structure changes with temperature. When operaing in multi-mode, the coherence length is approximately the length of the laser cavity, • 30 cm in our case. In order to circumvent the problem we designed and implemented a laser stabilization system. Figure 11 shows the longitudinal mode structure for long cavity laser. In this case, the central mode will experience the most gain and the laser will operate close to "single mode" and have a coherence length of 10s of meters. As temperature drifts cause the cavity length to change, the modes shift and two modes can be equally excited (as shown in Fig. 12) and the coherence length is reduced to cms. We designed a feedback system which controls the temperature of the laser tube in order to keep one mode in the center of the gain-bandwidth curve. Using this laser we were able to implement an 8-pass multi-pass cell, with about a 6 m path length difference demonstrating a long coherence length (see Fig. 13). However, the signal is somewhat weak because small reflections of laser power back into the laser cavity cause mode beating and destroys the laser mode structure. To get this under control an optical filter with 10% transmission was placed at the laser output. This greatly reduced the available power for the interferometer. Despite that, Figure 14 shows the phase noise of 50 ms acquisition. Here one sees a 60 Hz noise signal with amplitude of 10 degrees. If one zooms in to look at a 5 ms segment (the time frame of interest for the actual use of the instrument), the low frequency component appears as a straight line with a noise level of 1.2 degrees superposed (see Fig. 15).

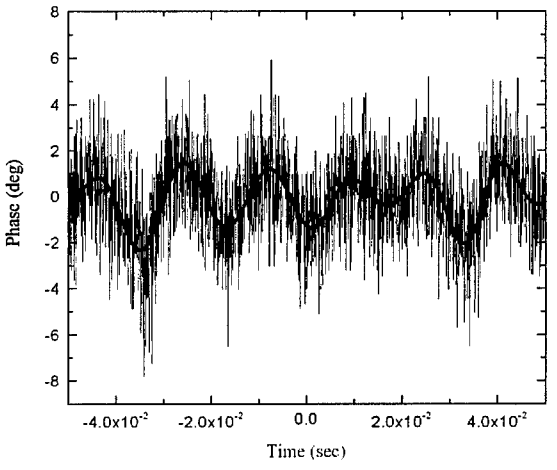

Figure 9. Phase noise with mis-matched Michelson setup using multi-mode laser exhibiting low noise levels.

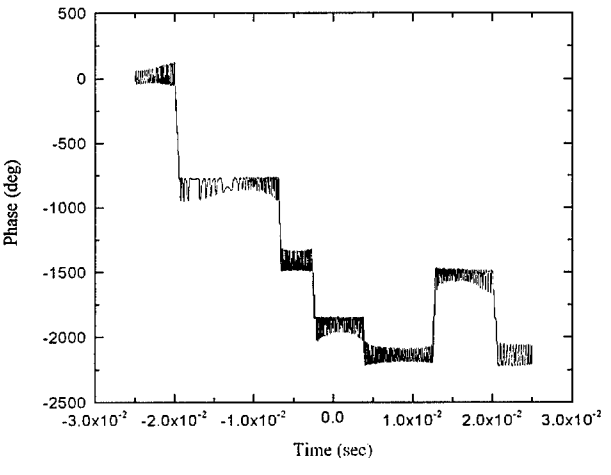

Figure 10. Next data capture using the same setup as in figure 1with far different results.

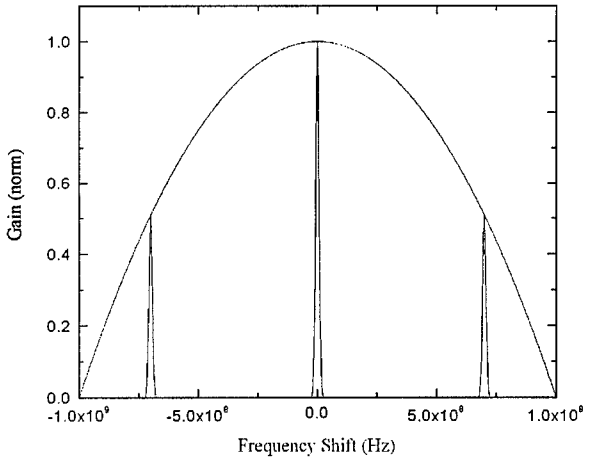

Figure 11. Gain-bandwidth diagram of the operation of a multi-mode laser.

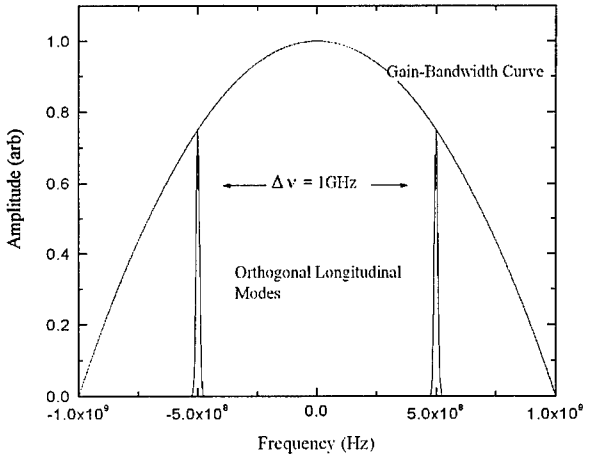

Figure 12. Gain-bandwidth diagram of a two mode laser (shorter laser cavity). By changing the cavity length (temperature tuning) the laser can be made to operate in a single longitudinal mode.

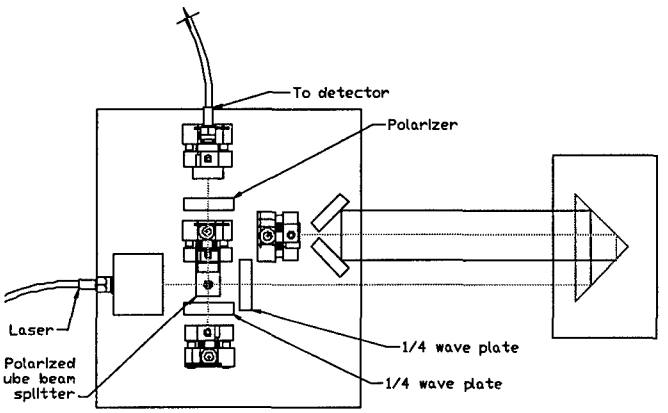

Figure 13. Detector head in a Michelson configuration with an eight pass detector arm (6 meters of path difference).

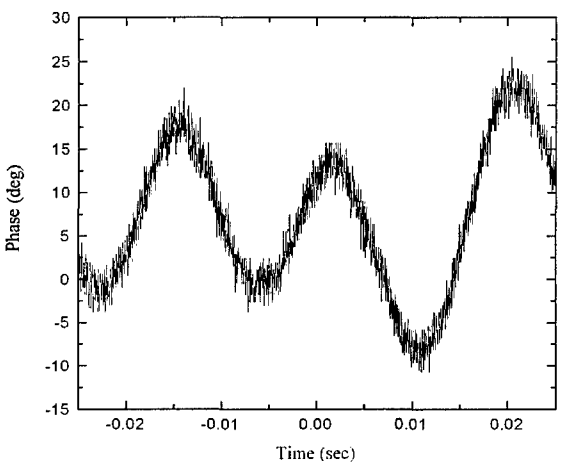

Figure 14. Phase noise for the above configuration using our temperature stabilized single mode HeNe laser.

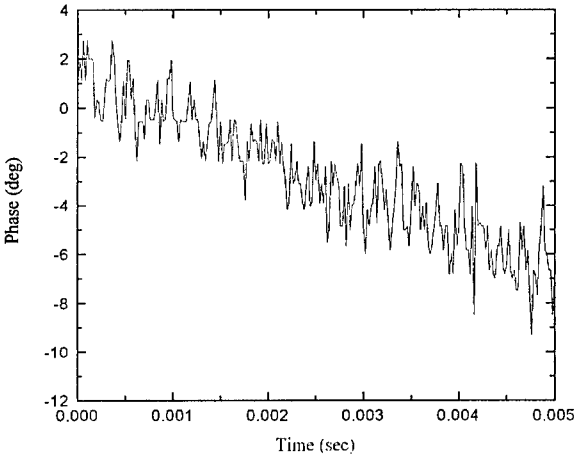

Figure 15. Five millisecond segment of the above data. The low frequency noise appears as a linear drift which feedback control can eliminate.

Two modifications were made to the optical system to improve its performance. The first was to add an optical isolator at the output of the stabilized laser to prevent reflected light from returning to the laser cavity and disrupting the mode operation. This was achieved previously by adding a substantial level of neutral density in the laser beam path at considerable expense to the detector signal levels. By adding the isolator, we could run at full power. The second was to add a half wave plate just prior to the insertion of the combined laser beams into the polarization-preserving fiber. This allows a more precise alignment of each component with its respective axis in the fiber. This minimizes mode mixing which would produce a phase error in the final analysis.

With these additional components, the multi-pass optical components were set up to produce an eight-pass test arm as shown in Fig. 16. The length of the arm is 75 cm, giving a total path length difference of 6 meters. The detector signal was strong and clean indicating that the stabilized laser was working well.

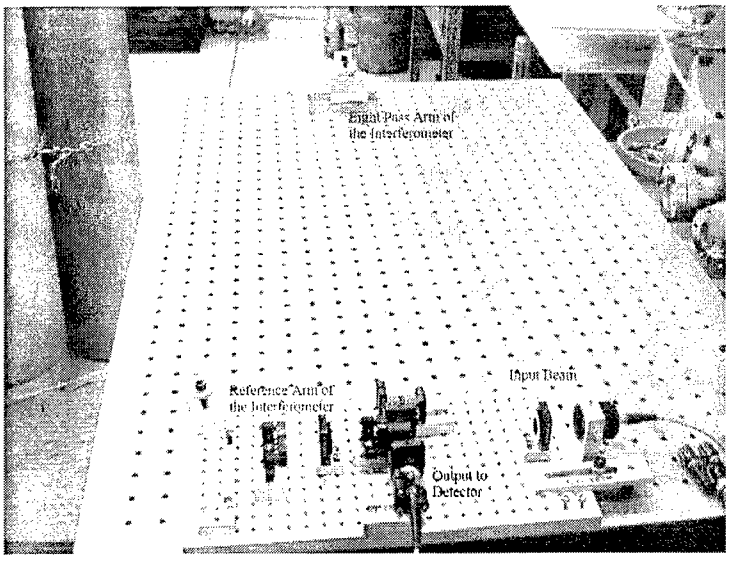

Figure 16. Interferometer head configured with an eight pass probe arm.

A number of test signals were acquired using this configuration. Figure 17 shows a 25 ms capture which exhibits a low frequency phase drift superposed on a high frequency noise. Using a two kHz FFT filter one can eliminate the high frequency component. If one captures a shorter time span (1ms) as shown in Fig. 4, one can eliminate the noise with a 50 kHz filters. This demonstrates that the oscilloscope sampling rate and not the actual frequency of the noise limits the bandwidth indicated in Fig. 18. Therefore, the addition of a physical low pass filter will eliminate the high frequency noise while, at the same time, preserving the bandwidth needed to properly resolve the gas puff rise.

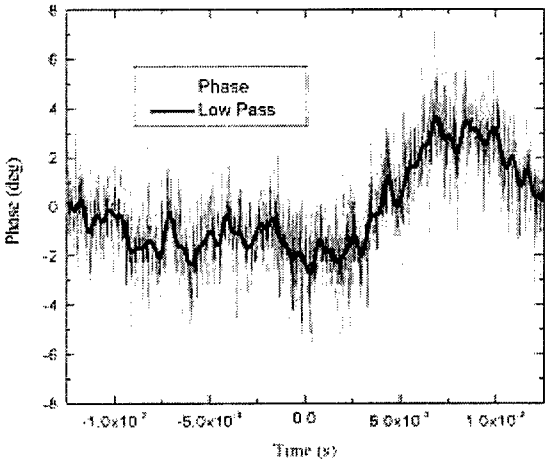

Figure 17. Phase noise during a 25 ms capture. High frequency filtered in software using a FFT low pass filter

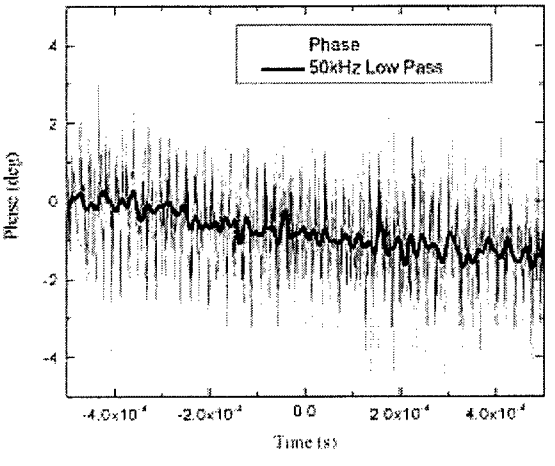

Figure 18. Phase noise during a 1 ms capture. Note that a 50 kHz filter effectivley removed the high frequency component.

As an initial test of the interferometer, a small amount of gas was pufffed into the sensor arm using a common laboratory duster. Figure 19 shows the response. Large phase shifts are easily tracked. Also there is enough resolution to measure the approximately 180• phase shift expected for the actual PRS load.

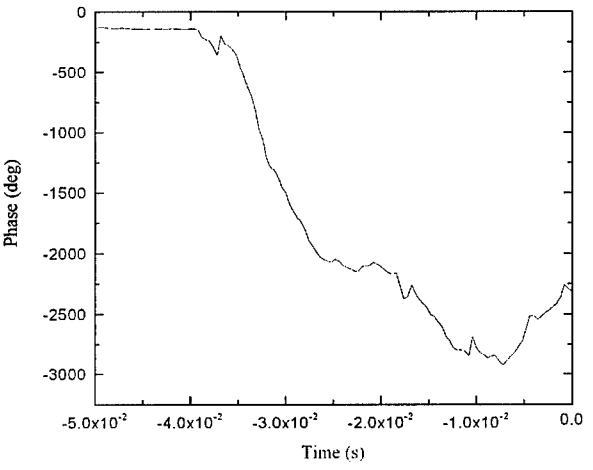

Figure 19. Interferometer response to a gas puff.

Measurements on Titan Puff Valve and Nozzle

The puff valve was received and installed in an HY-Tech vacuum chamber. Initial measurements were made with the vacuum chamber resting directly on the optical table upon which the interferometer is deployed. This showed a large vibration being transferred to the interferometer as could be seen in Fig. 20. In order to reduce the noise coupling, the puff valve and vacuum chamber were placed on a separate table spanning the interferometer table (see figs. 21 and 22). Figure 23 shows the substantial improvement in noise coupling. Note that the gas plenum had been depleted so that no gas was introduced during the cycling of the valve. The isolation is improved by approximately two orders of magnitude.

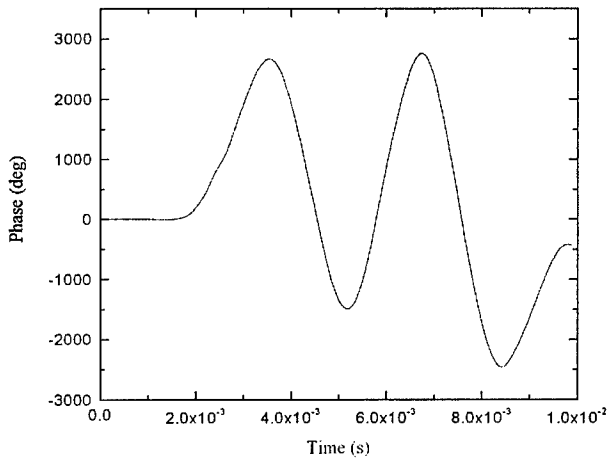

Figure 20. Phase noise induced with vacuum chamber housing puff valve sitting directly on the interferometer table.

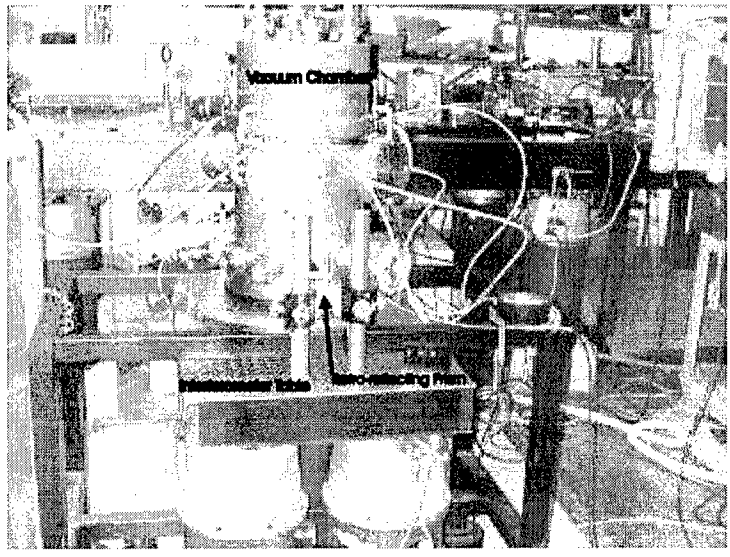

Figure 21. Vacuum chamber housing the puff valve suspended above the interferometer table viewed from the retroreflecting prism side.

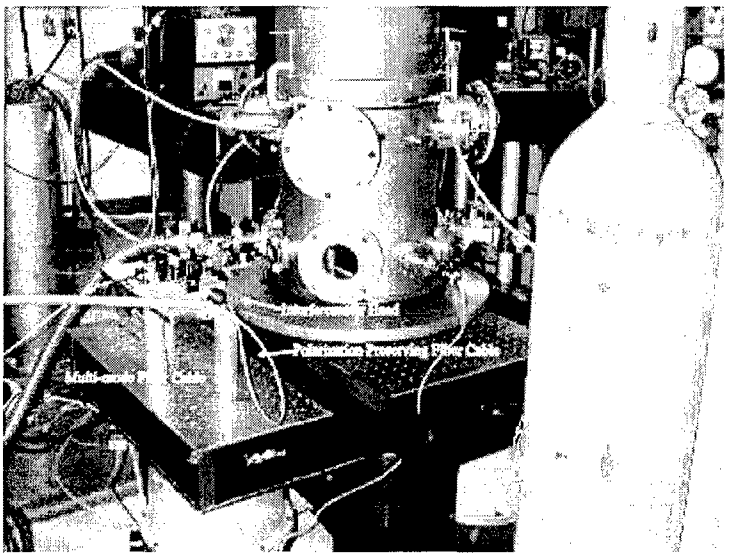

Figure 22. Vacuum chamber housing the puff valve suspended above the interferometer table viewed from the input side.

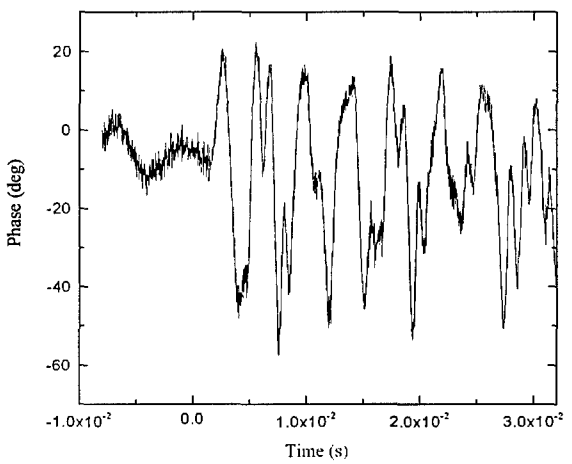

Figure 23. Phase noise induced with vacuum chamber housing puff valve suspended above the interferometer table.

The plenum was then pressurized with room air, and the effect of the gas was seen with the interferometer in a four pass configuration. (See Fig. 24) Here one can clearly see the rise of the gas density in about 2.4 ms. In figure 25 we increased to an eight pass cell and observed approximateley twice the phase shift. Assuming that the air is at room temperature and the gas is uniformly distributed in a 4 cm radius cylinder, one arrrives at

a peak mass loading of about 150 • g/cm, a vlaue on the order of the 100 • g/cm of argon expected on Double-EAGLE.

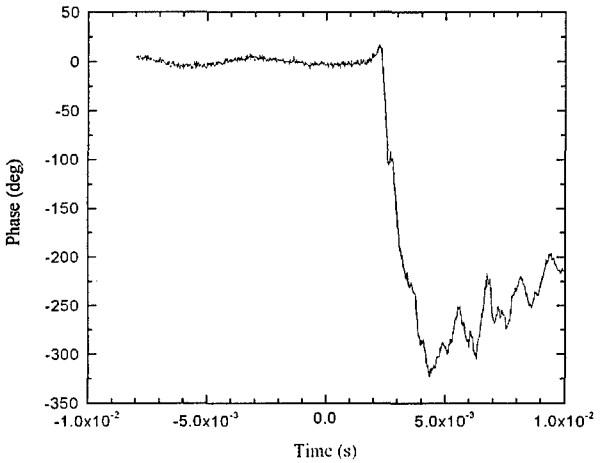

Figure 24. Phase measured for a gas puff of air at one atmosphere pressure using the interferometer in a four pass configuration.

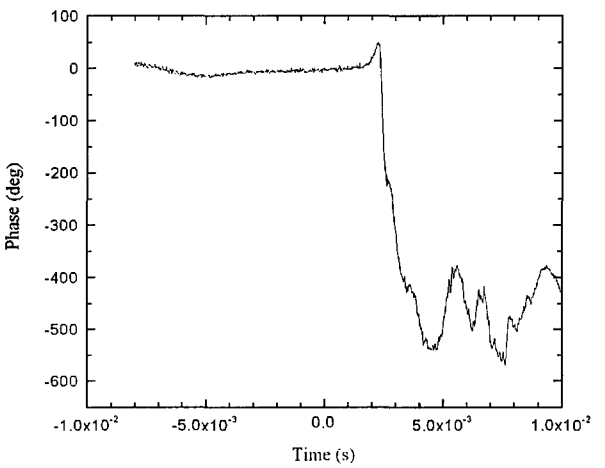

Figure 25. Phase measured for a gas puff of air at one atmosphere pressure using the interferometer in a eight pass configuration.

To further reduce the noise introduced by the valve, the valve mount in the vacuum chamber was isolated with a rubber absorber. With this improvement, the noise was essentially eliminated. The trigger pin driver box from Titan was installed and a series of

22 shots were made with a plenum pressure of six psia of argon. Figure 26 shows the jitter in the trigger pin signal relative to the triggering of the puff valve driver. Here one sees a jitter of about 100 • s. Figure 27 shows the corresponding phase signatures. Here one sees variations in both timing and amplitude. Figure 28 expands the region of interest at the beginning of the gas puff. There is a similar jitter of about 95 • s. However, if one adjusts the phase so that the trigger pin occurs at t=0, only a little improvement in the jitter is apparent, reducing to about 65• s. (see Fig. 29) Looking at the mass loading at 500 • s after the trigger signal (typical firing time for Double-EAGLE) the extremes vary • 22%. Figures 30 and 31 show the calculated mass loading values for each case with the standard deviation as error bars. Also included in the figure are lines showing the maximum excursions of the mass loading for the set of shots. These values are calculated by assuming that the gas is uniformly distributed in an 8-cm diameter cylinder. Similar calculations assuming two shells give a factor of 1.42 greater mass loading for the same measured phase. At the 500 • s point the standard deviations are about 12 %. Based upon these values a typical mass loading can vary up to 25 % shot to shot. Measurements made by Song et al. using the NRL interferometer for a 5 psia fill of argon, give a mass loading of 113 • 20.8 • g/cm. Their data show a linear relationship between plenum pressure and mass loading. Extrapolating their data to 6 psia gives a mass loading of 136 • g/cm, compared with our range of 116 to 145 • g/cm.

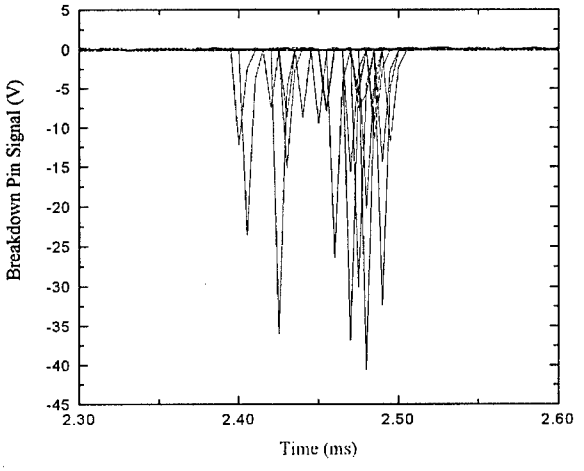

Figure 26. Jitter in breakdown pin output for 22 shots.

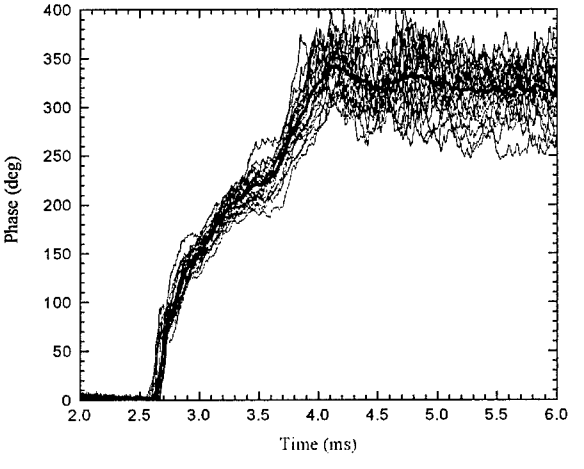

Figure 27. All 22 phase traces as recorded with eight-pass interferometer for a Titan 1234 nozzle pressurized at 6 psia of argon. Note the bold line in the center representing the average of all shots for this and subsequent figures.

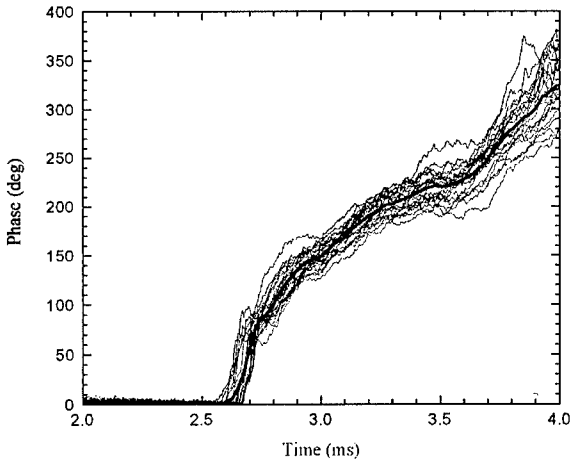

Figure 28. Expanded view of Figure 26 data.

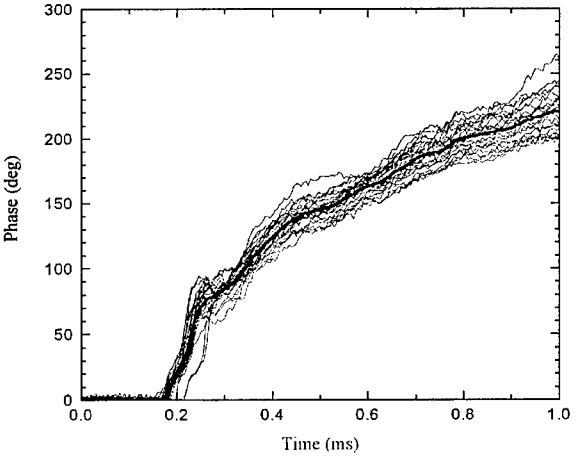

Figure 29. All 22 phase traces recorded with eight-pass interferometer for a Titan 1234 nozzle pressurized at 6 psia of argon with the timeing adjusted for breakdown pin jitter. The breakdown time was set to zero.

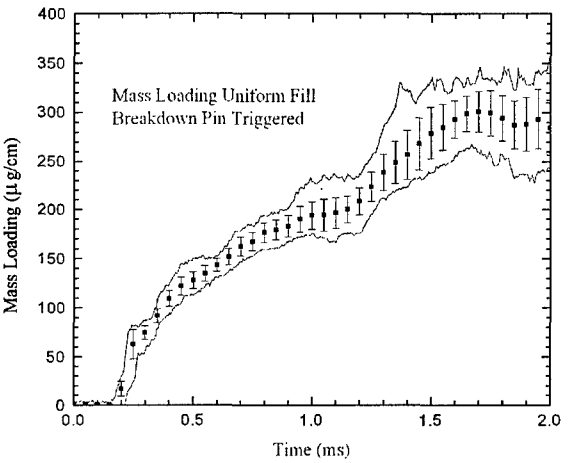

Figure 30. Statistics of mass loading measurements (assuming a uniform fill) adjusted for breakdown pin jitter. The error bars represent the standard deviation while the solid lines represent extrema of the measured values.

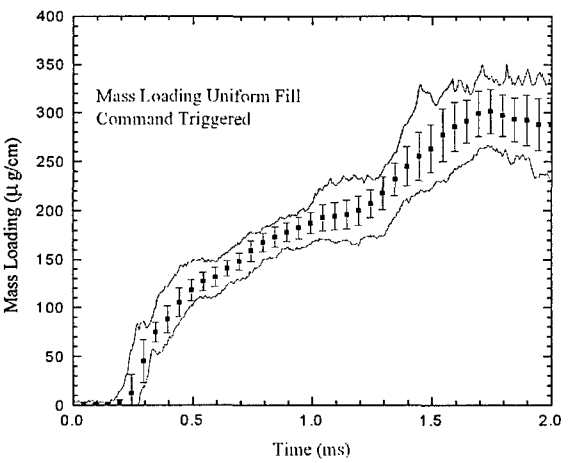

Figure 31. Statistics of mass loading measurements (assuming a uniform fill) not adjusted for breakdown pin jitter. The error bars represent the standard deviation while the solid lines represent extrema of the measured values. (This is essentially what one would see operating in a command trigger mode).

Trigger Electronics Tests

Having demonstrated the sensitivity to measure the gas puff phase, the next step is to derive a usable trigger signal. Due to long term drift effects the instantaneous phase measured at any point in time is essentially random. In order to generate a trigger signal the initial phase must be zero at the start of the gas puff. In a heterodyne interferometer a phase shift is manifested by an apparent frequency shift between the reference and scene beams. By replacing the Bragg cell driver frequency with one derived from a voltage controlled oscillator (VCO) a feedback or phase locked loop (pll) can be established which will maintain the output phase at zero. Such a pll was designed, fabricated and tested. In order to carry out the test in a quantifiable way, a solenoid driver was attached to the retro-reflecting prism in the multi pass optics. Using an audio oscillator as driver a consistent phase noise was introduced. Because of the nature of the heterodyne interferometer the conventional and pll controlled phase can be measured simultaneously.

Figure 32 shows the sinusoidal output from the conventional electronics. Here one sees an oscillation of about 250 degrees. In Fig. 33 the pll is periodically applied, resulting in segments of control and free oscillation. Here one can see that the phase is well zeroed, (• 1.3•, or about the digitizing level of the oscilloscope) demonstrating the effectiveness of the pll method.

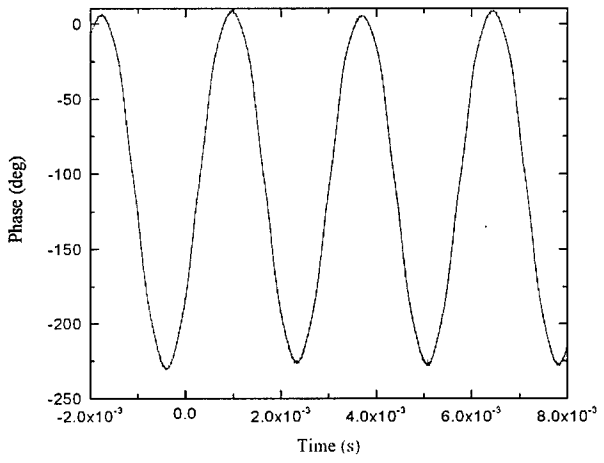

Figure 32. Phase signal measured with the retroreflector driven by an audio oscillator derived with conventional demodulation techniques.

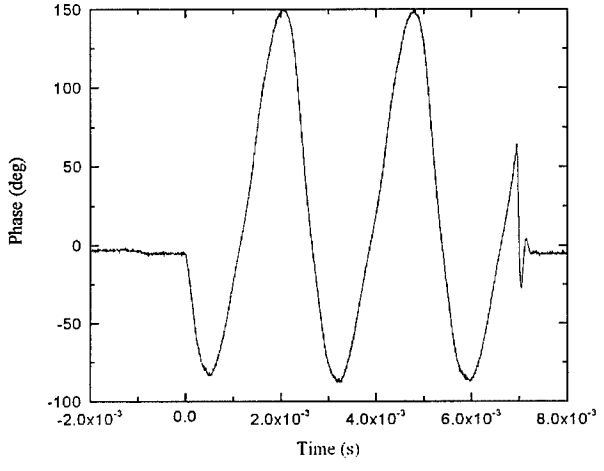

Figure 33. Phase signal measured with the retroreflector driven by an audio oscillator derived with phase locked loop demodulation techniques.

Discussion of Results

In the course of this Phase I effort we have met all of the technical objectives of the program. In order to be able to eventually use the system as a routine trigger source and as a mass loading and pre-ionization monitor, the heterodyne interferometer had to be fabricated in a manner that meet a set of criteria which would transform it from a sensitive laboratory tool into a robust, industrial sensor. These criteria broadly include:

immunity to environmental factors; non-interference with normal operations; ease of installation and use; modularity. In the process of developing this system, several technological barriers were encountered and overcome.

These measurements are in line with previous data derived using the NRL two-color interferometer which goes to extraordinary lengths, such as vacuum suspended mirrors, to eliminate vibrational noise to achieve the sensitivity needed to detect the index changes induced by the gas puff. Song et al. present data that show a variation in mass loading of about • 20% for conditions similar to ours. We show a standard deviation of • 11% and a range of • 22%. Both these measurements indicate that even with the use of the breakdown pin to trigger the shots, significant variations in mass loading still occur. The use of the interferometer trigger system will significantly improve the reproducibility and control of the mass loading. For simulators where data are acquired a few shots a day, this can greatly improve the quality of the data acquired and can remove a major variable in data analysis. There are a number of added benefits which can be derived from this system. First of all, not only does the system provide a measure of the mass loading at a fixed axial position at a fixed time (the effective trigger point), it also can provide a measure of the axial mass distribution for each shot. Second, the device should be sensitive enough to measure the pre-ionization level on each shot, allowing one to determine the effect of any variations therein. Finally, the system will be able to measure the early stages of electron build up in the breakdown phase of the discharge.